

OVERDAMPED DYNAMICS IN SEPTATE CHANNELS*

MARCELLO BORRROMEO

Dipartimento di Fisica, Università degli Studi di Perugia
and

INFN — Sezione di Perugia, Via A. Pascoli, 06123 Perugia, Italia

(Received April 11, 2013)

I summarize recent results on Brownian transport in hard-geometry compartmentalized channel, investigating mobility and diffusion as functions of the driving force and the geometry of the cells. Numerical calculations are performed using parallel algorithms on graphics cards. The large drive limit can be fairly well understood in terms of transverse diffusion, while the low drive one can be explained using renewal theory or the random walker jump approximation.

DOI:10.5506/APhysPolB.44.1037

PACS numbers: 05.10.Gg, 05.40.-a

1. Outline

Diffusion in periodic channels has gained much interest lately [1], because of the many possible applications, both in explaining natural phenomena [2] and in building nanotechnological devices [3]. Channels are naturally found in zeolites [4], porous stones with a regular inner structure, and can be built and modelled artificially. The study of these systems can be performed both analytically, starting from the Fokker–Planck equation, mainly when the channels have smooth boundaries, or numerically, relying on the Langevin equation, and possibly exploiting the parallel behaviour of the problem.

This paper is organized as follows: the first section will deal with different types of channels and their physical role, in the second three types of septate channels will be introduced, in the third the behaviour of mobility and diffusion will be shown for periodic channels, in the fourth for non-periodic channels, and, finally, in the fifth section, numerical methods used for simulations, namely massively parallel computations on graphics cards, will be described.

* Presented at the XXV Marian Smoluchowski Symposium on Statistical Physics, ‘Fluctuation Relations in Nonequilibrium Regime’, Kraków, Poland, September 10–13, 2012.

2. Channels

Channels are widespread in physics and biology, appearing in cell ionic channels, in porous materials and in many other fields of science; here, I will restrict myself to compartmentalized channels, that is channels made up with basic blocks, cells, that look all more or less the same. I will further assume that motion is in the x -direction, while the y - and z -directions (in planar and three dimensional space) are limited by boundaries. If the system is planar, and the cell symmetric with respect to y -axis inversion, the boundaries can be described by a positive function $w(x)$; the motion is then restricted to points (x, y) that satisfy $|y| < w(x)$.

The analytic treatment of the problem is simplified if $w(x)$ satisfies the smoothness condition

$$w'(x) < 1.$$

In this case, the y - and, eventually, z -variables can be averaged out in the Fokker–Planck equation and we get the Fick–Jacobs equation [5–7]

$$\frac{\partial P(x, t)}{\partial t} = D_0 \frac{\partial}{\partial x} \left(w(x) \frac{\partial P(x, t)}{\partial x} \frac{1}{w(x)} \right).$$

Such channels allow interpreting the quantity $k_B \ln(w(x))$ as an entropy and are thus named entropic channels (Fig. 1 (a)) [8–10]. When this condition does not hold, we have to face the full Fokker–Planck equation or to solve the problem by numerical simulation: we are then dealing with septate channels (Fig. 1 (b)) [11–13].

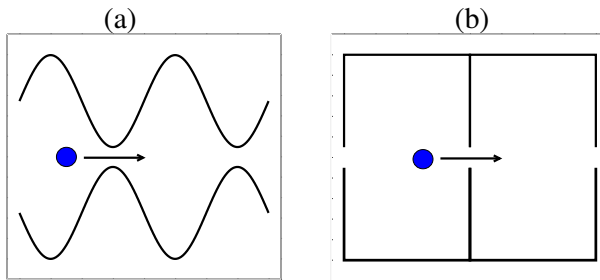


Fig. 1. Two types of cells: (a) with smooth boundaries (entropic cell) (b) with hard boundaries (septate cell).

3. Septate channels

I will study here planar rectangular channel cells with sides x_L and y_L and openings (pores) of amplitude Δ on the y -side. The dynamics of particles in these compartments changes depending on where the openings are precisely placed. Three cases will be considered [14, 15]:

1. all the cells are identical, and the openings are centred in the y -side (periodic, Fig. 2 (a));
2. there are two types of cells alternating with the openings shifted up and down respectively of the same amount y_H (alternate, Fig. 2 (b));
3. the cells are all different, and the openings are randomly set with the center displaced with respect to the x -axis by an amount y_H distributed according to a truncated Gaussian with standard deviation σ (random, Fig. 2 (c)).

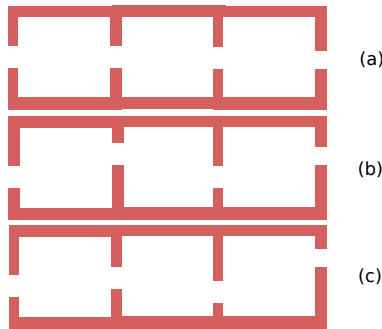


Fig. 2. Different types of septate channels: (a) periodic; (b) alternate; (c) random.

3.1. Periodic channels

I first consider channels made of identical cells, with an aperture of amplitude Δ centred on the y -axis. A particle subject to a constant drive F along the x -axis, starting in the central lane, will be able to travel across cells even in absence of noise. Adding white Gaussian noise in both directions, and assuming that the motion is overdamped, we get the Langevin equations

$$\frac{dx}{dt} = F + \sqrt{2D_0} \xi_x(t), \quad \frac{dy}{dt} = \sqrt{2D_0} \xi_y(t), \quad \langle \xi_i(t) \cdot \xi_j(t') \rangle = \delta_{ij} \delta(t - t').$$

The equations can be rescaled by setting $t = \bar{t}/D_0$ and $f = F/D_0$, so that

$$\frac{dx}{d\bar{t}} = f + \sqrt{2} \xi_x(\bar{t}), \quad \frac{dy}{d\bar{t}} = \sqrt{2} \xi_y(\bar{t}), \quad \langle \xi_i(\bar{t}) \cdot \xi_j(\bar{t}') \rangle = \delta_{ij} \delta(\bar{t} - \bar{t}').$$

This shows that, provided that time is measured in units of $1/D_0$, the physical quantities can only depend on F/D_0 .

The model is completely specified only when the properties of the boundaries are fixed: here we assume they are perfectly reflecting.

In the following, I will study the behaviour of mobility and diffusion as functions of the compartment geometry and of the driving f .

3.2. Mobility

In figure 3, we show the mobility

$$\mu(F) = \lim_{t \rightarrow \infty} \frac{\langle x(F, t) - x_0 \rangle}{t \cdot F}$$

as a function of F/D_0 , for different values of the cell length. Three main conclusion can be drawn from the results:

1. There is a finite limit, dependent on x_L , for $F/D_0 \rightarrow 0$;
2. There is a plateau, independent on x_L , for large drives;
3. The plateau is approached with an approximate law

$$\mu - \mu_\infty \sim F^{-1/2}.$$

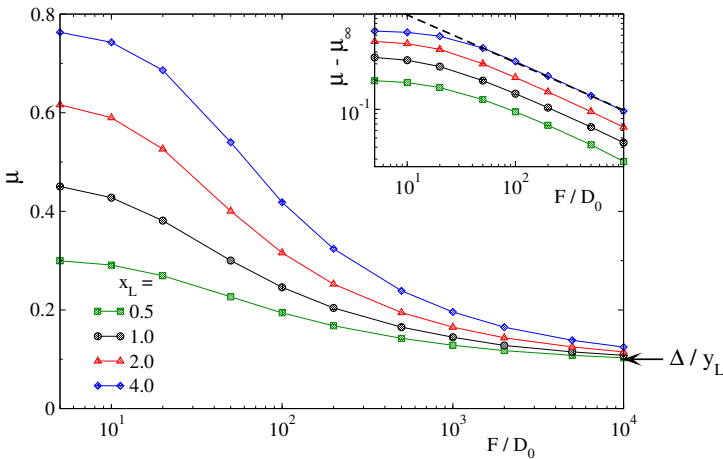


Fig. 3. Mobility as a function of F/D_0 for $y_L = 1$, $\Delta = 0.1$, $D_0 = 0.05$ and different values of x_L . Inset: The same with $\mu - \mu_\infty$ plotted on the y -axis, instead of μ .

I will postpone the explanation of the first point since this is based on the relation [16]

$$\mu_0 = \mu(F = 0) = D(F = 0)/D_0$$

and will be discussed together with the diffusion.

The second point can be understood considering, as shown in Fig. 4, what happens when the drive becomes very large: the time needed to cross the cell will be very small compared to the time employed to diffuse transversely and reach the central opening; therefore, on average, only a fraction Δ/y_L of particles will be in the central channel, moving with speed F . This gives the large drive mobility independent on x_L [11–13].

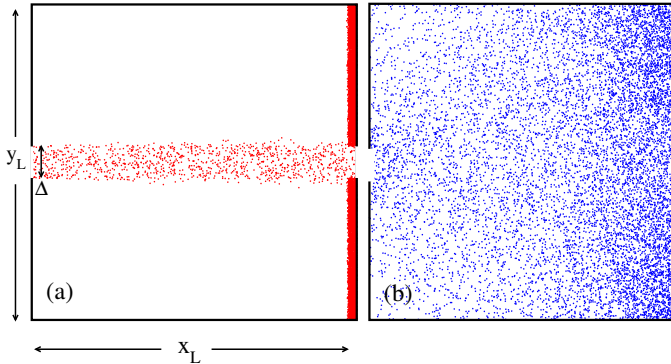


Fig. 4. Distribution of $N = 10000$ particles for $x_L = y_L = 1$, $D_0 = 0.05$, $\Delta = 0.1$ for (a) $F/D_0 = 10000$ and (b) $F/D_0 = 5$.

In figure 5, the dependence on the aperture amplitude Δ is shown. We see that it depends logarithmically on the aperture amplitude. For small Δ , we can assume that the process is a random motion of a walker jumping between pores, with a mean first passage time τ_0 , and the mobility is

$$\mu(0) = \frac{x_L^2}{2D_0\tau_0}.$$

An approximate value for τ_0 can be analytically calculated by a variety of techniques [11, 15, 17, 18] and reads

$$\mu(\Delta) = \frac{\mu(y_L)}{1 - \frac{2}{\pi} \frac{y_L}{x_L} \ln\left(\frac{\Delta}{y_L}\right)}.$$

This estimate of $\mu(\Delta)$ holds good for small Δ , while it fails for larger values, when the random jumper description is not appropriate. The conditions of equivalence between the discrete random jumper scheme and the entropic Fick–Jacobs scheme are discussed in [19].

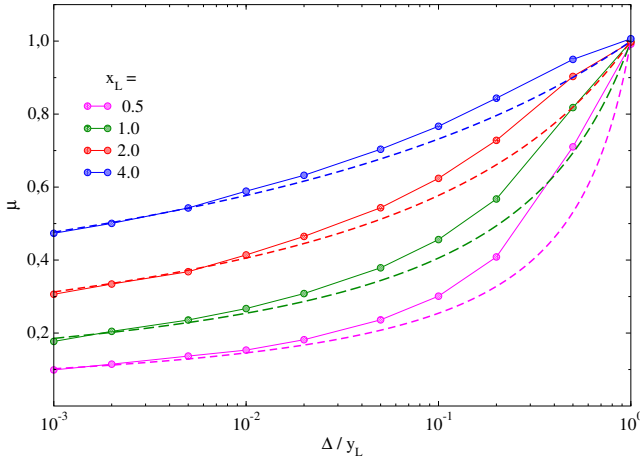


Fig. 5. Mobility *vs* aperture amplitude Δ for $y_v s = 1$, $F = 0$, $D_0 = 0.05$ and several values of $x_v s$. The dashed lines are the analytic formulae.

3.3. Diffusivity

Diffusivity

$$D(F) = \lim_{t \rightarrow \infty} \frac{\langle (x(F, t) - \langle x(F, t) \rangle)^2 \rangle}{2t}$$

as a function of the driving force is shown in Fig. 6. We see that, unlike what happens with entropic cells, the large drive limit is not the free particle diffusion and that there is no diffusion peak, but a monotonic behaviour. For large drives and small Δ , the system switches between running and

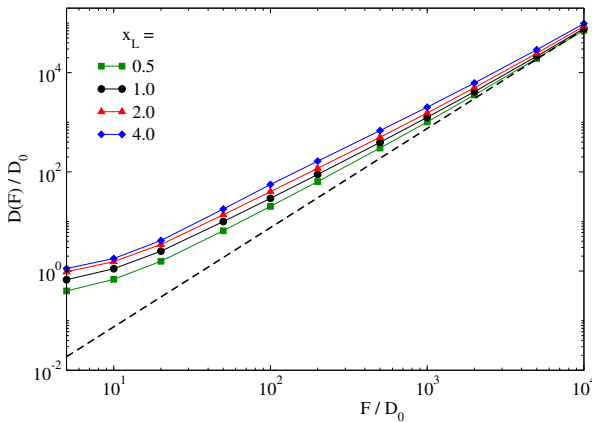


Fig. 6. Diffusivity as a function of F/D_0 for several values of x_L and $y_L = 1$, $\Delta = 0.1$, $D_0 = 0.05$.

locked states, the last ones slowly diffusing along the y -axis. Accordingly, the particle velocity can be modelled by a dichotomous signal; its diffusivity is given by [15]

$$\frac{D}{D_0} = \frac{\Delta^2}{12} \left(1 - \frac{\Delta}{y_L}\right)^3 \left(\frac{F}{D_0}\right)^2.$$

4. Non-periodic channels

Using the ideas developed for periodic channel, we examine now two types of non-periodic channels: alternate channels, where the centre of the aperture is shifted alternatively up and down by a fixed amount y_H , and random channels, where y_H is a random variable with truncated Gaussian distribution [14].

4.1. Channels with alternate cells

If $y_H > \Delta/2$ the central lane is blocked and, for large drives, almost all of the time is spent diffusing on the y -axis (Fig. 7). This behaviour can be described as a renewal process and, using the first two moments of $P(\tau)$, $\langle\tau\rangle$ and $\langle\tau^2\rangle$, we get

$$\mu(F) = \frac{x_L}{F \cdot \langle\tau\rangle}, \quad D(F) = \frac{x_L^2}{2} \cdot \frac{\langle\tau^2\rangle - \langle\tau\rangle^2}{\langle\tau\rangle^3}.$$

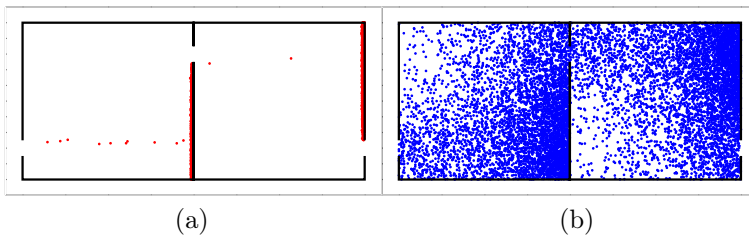


Fig. 7. Distribution of $N = 5000$ particles moving in alternate cells for (a) $F/D_0 = 5$ and (b) $F/D_0 = 5$, $x_L = y_L = 1$, $D_0 = 0.05$ and $\Delta = 0.1$.

Since the particles are bound to move in a small strip around the cell border, their motion can be considered one-dimensional; the moments can be computed considering the problem of the mean exit time from an interval with one reflecting and one absorbing barrier, leading to the result [20]

$$\mu = \frac{y_L}{2y_H - \Delta} \left(\frac{2x_L}{y_L^2}\right) \frac{D_0}{F}, \quad \frac{D(F)}{D_0} = \left[1 + \left(\frac{y_L}{2y_H - \Delta}\right)^2\right] \frac{x_L^2}{3y_L^2}.$$

A comparison between theory and numerical simulations is shown in figures 8 and 9. Our theory describes well large F decay of both diffusion and mobility.

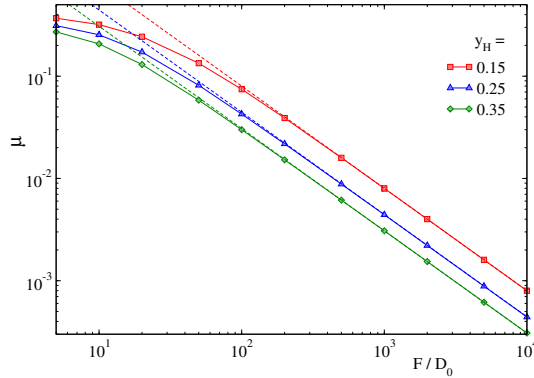


Fig. 8. Mobility in channels with alternate pores with $\Delta = 0.05$, $D_0 = 0.05$, $x_L = y_L = 1$.

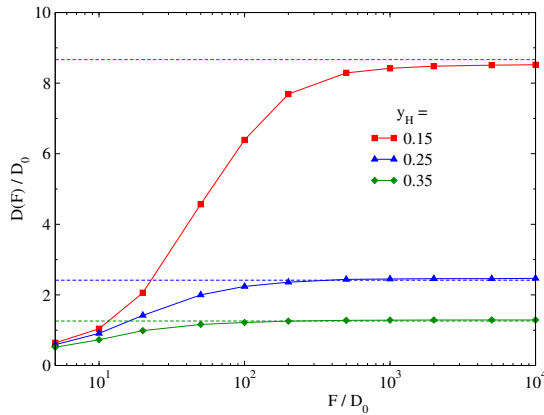


Fig. 9. Diffusivity in alternate channels averaged over 10^4 trajectories, with $\Delta = 0.10$, $D_0 = 0.05$, $x_L = y_L = 1$.

4.2. Random channels

If we take randomly the position of the aperture centre in the interval $[-y_L + \Delta/2, y_L - \Delta/2]$ with Gaussian probability, the situation is a mix of the two previous cases: for small values of the standard deviation σ the cells will look almost as periodic, while for large values the central lane will be closed

and y -diffusion will dominate. What we expect is therefore that, for small σ (Fig. 10 (a)), there will be a resemblance with periodic channels whereas, for large σ (Fig. 10 (b)), the problem will be rather similar to alternate cells.

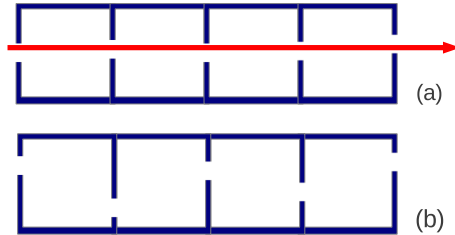


Fig. 10. Random channels (a) σ small (b) σ large.

What we see in fact is that, for large F , the mobility approaches a constant value at small σ , and drops to zero with a power law for large σ . Similarly, the diffusion diverges for small σ and large F while it reaches an asymptote for large σ . Results for random channels are shown in Fig. 11

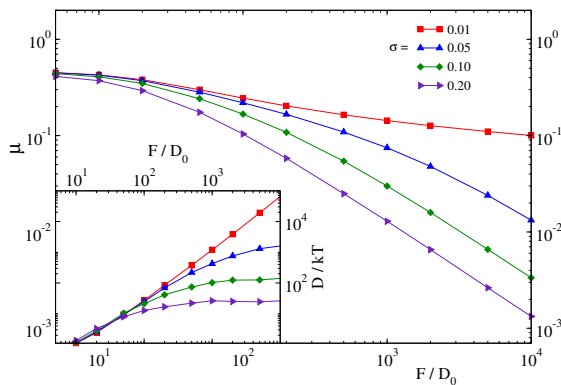


Fig. 11. Mobility and diffusion (inset) for random channels averaged over 10^3 trajectories with $D_0 = 0.05$, $\Delta = 0.05$ and $x_L = y_L = 1$.

5. Numerical methods

Numerical computations can be considerably sped up if we consider that we want to calculate averages over many particles, and we can assume that all these particles evolve during the same time interval. Moreover, in the present description, all particles are independent of one another, and the simulations can be performed in parallel. There are presently several choices to perform such computations, two of them being computations distributed over a network grid and over a computer cluster using MPI. In

the present work, I used the capability of recent graphics cards, made of hundreds or thousands of processors, to perform parallel calculations using the CUDA [21] extension to the C programming language. The basic idea is that every processor in the Graphics Processing Unit (GPU) can be used for simple tasks, so we can employ it for advancing one time step for a single particle in numerical integration. Since several thousands of threads are allowed simultaneously, many particles can be advanced of one time step simultaneously, considerably reducing the computation time. In practice, the Central Processing Unit (CPU) gives control to the GPU for the time needed to perform, in parallel, a simple operation, and the result is then copied back to the CPU. The operation is then repeated for the next time step, as many times as needed. A flow diagram of the code is shown in Fig. 12

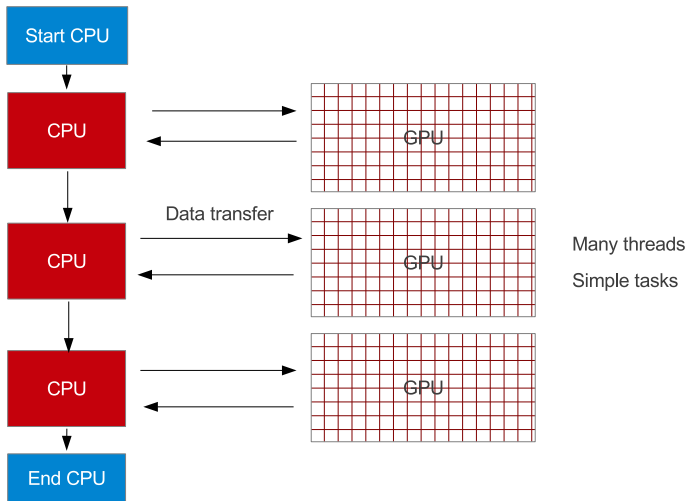


Fig. 12. Scheme of a program running on a GPU.

6. Conclusions

I have been studying overdamped motion in septate channels made of cells with different shapes. Their behaviour is quite different from entropic channels and depends on the geometry: for periodic channels we find a finite large- F mobility asymptote and a diverging diffusivity, while, in the same limit, alternate channels display a mobility vanishing like $1/F$ and a diffusivity reaching an asymptote. Finally, random channels switch between the two behaviours by increasing σ .

All calculations were performed using GPU computing capabilities.

REFERENCES

- [1] P.S. Burada *et al.*, *Chem. Phys. Chem.* **10**, 45 (2009).
- [2] B. Hille, *Ion Channels of Excitable Membranes*, Sinauer, Sunderland, 2001, Chap. 1 and following; H. Brenner, D.A. Edwards, *Macrotransport Processes*, Butterworth-Heinemann, New York 1993.
- [3] P. Hänggi, F. Marchesoni, *Rev. Mod. Phys.* **81**, 387 (2009).
- [4] J. Kärger, D.M. Ruthven, *Diffusion in Zeolites and Other Microporous Solids*, Wiley, New York 1992.
- [5] M.H. Jacobs, *Diffusion Processes*, Springer, New York 1967.
- [6] R. Zwanzig, *J. Phys. Chem.* **96**, 342 (1992).
- [7] D. Reguera, J.M. Rubi, *Phys. Rev.* **E64**, 061106 (2001).
- [8] P. Kalinay, J.K. Percus, *Phys. Rev.* **E74**, 041203 (2006).
- [9] N. Laachi, M. Kenward, E. Yariv, K.D. Dorfman, *Eur. Phys. Lett.* **80**, 50009 (2007).
- [10] P.S. Burada *et al.*, *Phys. Rev.* **E75**, 051111 (2007).
- [11] A.M. Berezhovskii, A.V. Barzykin, V.Yu. Zitserman, *J. Chem. Phys.* **132**, 221104 (2010).
- [12] F. Marchesoni, S. Savelev, *Phys. Rev.* **E80**, 011120 (2009).
- [13] F. Marchesoni, *J. Chem. Phys.* **132**, 166101 (2010); *J. Chem. Phys.* **131**, 224110 (2009).
- [14] M. Borromeo, F. Marchesoni, P.K. Ghosh, *J. Chem. Phys.* **134**, 051101 (2011).
- [15] M. Borromeo, F. Marchesoni, *Chem. Phys.* **375**, 536 (2010).
- [16] H. Risken, *The Fokker–Planck Equation*, Springer-Verlag, Berlin 1989, p. 342.
- [17] F. Sauli, CERN internal note 77-09, 1977.
- [18] A. Singer, Z. Schuss, D. Holcman, R. S. Eisenberg, *J. Stat. Phys.* **122**, 437 (2006); A. Singer, Z. Schuss, D. Holcman, *J. Stat. Phys.* **122**, 465 (2006); *J. Stat. Phys.* **122**, 491 (2006).
- [19] L. Bosi, P.K. Ghosh, F. Marchesoni, *J. Chem. Phys.* **137**, 174110 (2012).
- [20] S. Redner, *A Guide to First-Passage Processes*, Cambridge University Press, 2001.
- [21] For an introduction see: J. Sanders, E. Kandrot, *CUDA by Example: An Introduction to General-Purpose GPU Programming*, Addison–Wesley, 2010.